Earth and Planetary Science Letters 300 (2010) 264–274

Contents lists available at ScienceDirect

Earth and Planetary Science Letters

journal homepage: www.elsevier.com/locate/epsl

Modelling melting rates in upwelling mantle

Ian J. Hewitt

Department of Mathematics, University of British Columbia, #121 1984 Mathematics Rd, Vancouver BC, V6T 1Z1, Canada

ARTICLE INFO

Article history:
Received 29 June 2010
Received in revised form 30 September 2010
Accepted 6 October 2010
Available online 6 November 2010

Editor: Y. Ricard

Keywords:
partial melting
reactive infiltration
melt channels
magma
mid-ocean ridge

ABSTRACT

Upwelling regions of the mantle can undergo partial melting as a result of decompression. Many models for the dynamics of these regions have largely ignored the actual melting process or have prescribed a uniform melting rate proportional to the upwelling velocity. This paper uses a simple model for an upwelling column to calculate the melting rate from conservation principles. The model rock comprises two chemical components, and is assumed to be in thermodynamic equilibrium. For idealized linear phase constraints the melting rate can be calculated analytically, and is found to be proportional to the average upwelling velocity of both the matrix and melt.

A secondary aim is to discuss reactive instabilities; the model predicts that the one dimensional state will be linearly stable, whereas previous models have suggested that reactive infiltration instability should occur. This is argued to be a result of the 'background' melting rate which has not usually been fully accounted for, but which has a stabilizing effect. The model here can also be applied to a column in which some melt is already present, and in that case it does exhibit a channeling instability. It is concluded that accounting for melt production consistently in mid-ocean ridge models is important when assessing the likely modes of melt transport.

1. Introduction

Magma is produced in upwelling regions of the mantle by decompression melting: hot rock that ascends as a result of large scale mantle convection is forced to partially melt when it intersects its pressure dependent solidus (Fig. 1b). Melt is produced at the grain boundaries, which form a permeable network that allows the melt to rise as a result of its buoyancy (Turcotte and Ahern, 1978). Porous flow is thought to be sufficiently slow that chemical equilibrium should be effectively maintained between the ascending melt and the residual solid matrix. This disagrees with inferences from geochemistry that erupted melts are often in disequilibrium with the residual rock through which they travelled, and suggests that there must be faster, chemically isolated, means of melt transport (Kelemen et al., 1997). This observation has motivated a number of fluid mechanical studies to understand how melt flow organizes itself, and how it influences the geochemistry.

Most models have followed the formulation of McKenzie (1984), who set out what have become known as compaction equations, due to the viscous compaction of the matrix that distinguishes the situation from more standard models of porous flow (Drew, 1983). Notable topics of study have included travelling compaction waves (eg. Scott et al., 1986), decompaction channels (Sparks and Parmentier, 1991; Spiegelman, 1993), formation of shear bands (Stevenson, 1989), and formation of channels by reactive infiltration (Aharonov et al., 1995; Kelemen et al., 1995). Most of these studies have ignored the actual melt production process, however, and focused on the movement of melt that is somehow already present in the rock. The present paper aims to include the melting process in a consistent manner and to look at some of the implications of doing so, particularly with regard to reactive channel formation.

Several authors have included melting in one dimensional solutions (Hewitt and Fowler, 2008; Ribe, 1985b; Šrámek et al., 2007; Turcotte and Ahern, 1978), but until recently most two dimensional models have either ignored it or have *prescribed* a melting rate in order to achieve a desired degree of melting (Choblet and Parmentier, 2001; Ribe, 1985a; Scott and Stevenson, 1989; Spiegelman et al., 2001) (notable exceptions are Katz (2008), who used an enthalpy method to calculate the melting rate implicitly, and Hewitt and Fowler (2009), who calculated melting rates but only for a single component rock).

The approach we take here follows very closely that used by Ribe (1985b) and adopted also by Katz (2008); we assume that the mantle rock is made up of just two components, and that the matrix and melt are everywhere in thermodynamic equilibrium. This imposes phase constraints on the temperature and composition of the rock which, together with conservation laws, determine how fast it melts.

The intention is not to improve on the *accuracy* of existing models for melt production; there are considerably more complete thermodynamical treatments that involve parameterized melt transport (Asimow et al., 1997; Asimow and Stolper, 1999; Ito and Mahoney, 2005; McKenzie and Bickle, 1988; Stolper and Asimow, 2007). The intention is rather to incorporate a consistent description of the melting process within a fluid dynamical model, in the hope that we at least capture its phenomenological effect on the melt flow.

Section 2 describes the simplest possible model that includes the essential ingredients of mass, momentum and energy conservation.

E-mail address: hewitt@math.ubc.ca.

0012-821X/$ – see front matter © 2010 Elsevier B.V. All rights reserved.
doi:10.1016/j.epsl.2010.10.010

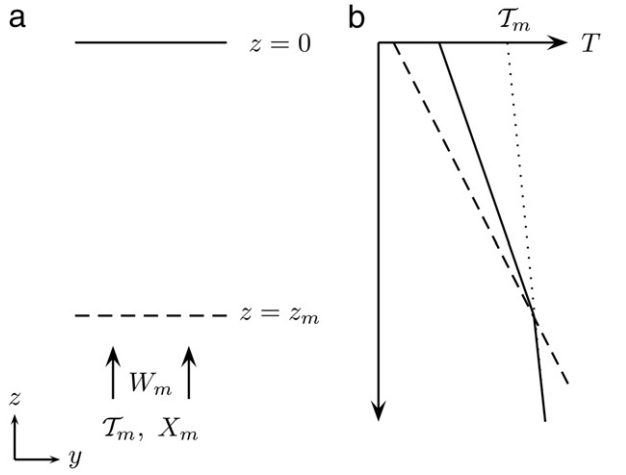

Fig. 1. (a) The model column of rock is fed by a uniform supply from below moving with vertical velocity W_m, having potential temperature $\mathcal{T}_m$ and composition X_m. (b) The dotted line shows the adiabatic temperature profile and the dashed line shows the pressure dependent solidus for the initial composition X_m. Above the intersection at z_m, melting occurs and the rock follows the solidus (solid line), which varies with both pressure and composition as the rock melts (see also the solutions to the equations shown in Fig. 3).

Section 3 reviews the one dimensional solutions, and introduces a particular form of linear phase constraint that allows the melting rate to be calculated analytically. In Section 4, we use these phase constraints to calculate the melting rate more generally in two or three dimensions, and notice how this relates to simplified rates that have been assumed in the past.

The calculated melting rate can be split into components due to the ascending matrix and the ascending melt. If there is a sufficient quantity of melt this may lead to a reactive instability as a result of the positive feedback between melting rate and melt flow (Ortoleva et al., 1987). This is examined in Section 5, and there is further discussion of the implications and limitations of this model in Section 6. We find that instability depends upon the background steady state, and that it is therefore important to consider the entire melting process in order to determine whether channelization is likely to occur.

2. Model

2.1. Model setup

The situation we consider throughout the paper is a column of rock that is ascending as a result of the larger scale convective motion of the mantle (Fig. 1). This prescribes boundary conditions on the rock at the bottom of the column: it is ascending with *upwelling* velocity W_m, it has known potential temperature[1] $\mathcal{T}_m$, and known composition X_m (the rock is assumed to comprise two components, with fraction X_m and $(1-X_m)$ respectively. These are treated hypothetically, but might represent, for instance, fayalite Fe_2SiO_4 and forsterite Mg_2SiO_4, which make up olivine).

The adiabatically ascending rock intersects its solidus at a depth denoted z_m, above which partial melting is assumed to continue all the way to the surface $z=0$ where the pressure is atmospheric. Note that the one dimensionality of the upwelling means that the rock apparently continues to ascend through the surface $z=0$; in reality it should spread sideways near the surface and there should be a cold conductive boundary layer making up the lithosphere. The melt that reaches the lithosphere may refreeze, or collect in a magma chamber, or erupt to create new crust, but these considerations are beyond the scope of this paper. We simply assume that melting continues to the surface, and that the amount and composition of melt there may be indicative of 'erupted' melts.

2.2. Thermodynamic equilibrium

The model assumes thermodynamic equilibrium; that is, melting occurs sufficiently fast that the temperature and composition of the rock are constrained by its solidus and liquidus curves. These are taken to be given by

$$T_S = T_{S0} + \gamma p_s + \lambda f_S(X_s), \tag{1}$$

$$T_L = T_{L0} + \gamma p_s + \lambda f_L(X_l), \tag{2}$$

where T_{S0} and T_{L0} are reference temperatures, $p_s = -\rho g z$ is the lithostatic pressure due to density ρ and gravity g, γ is the Clapeyron slope (assumed constant), λ is the temperature variation due to changes in composition, and f_S and f_L are order one functions of the solid composition X_s and liquid composition X_l. Example surfaces for the solidus T_S and liquidus T_L are shown as functions of pressure and composition in Figure 2a. In thermodynamic equilibrium, the liquid

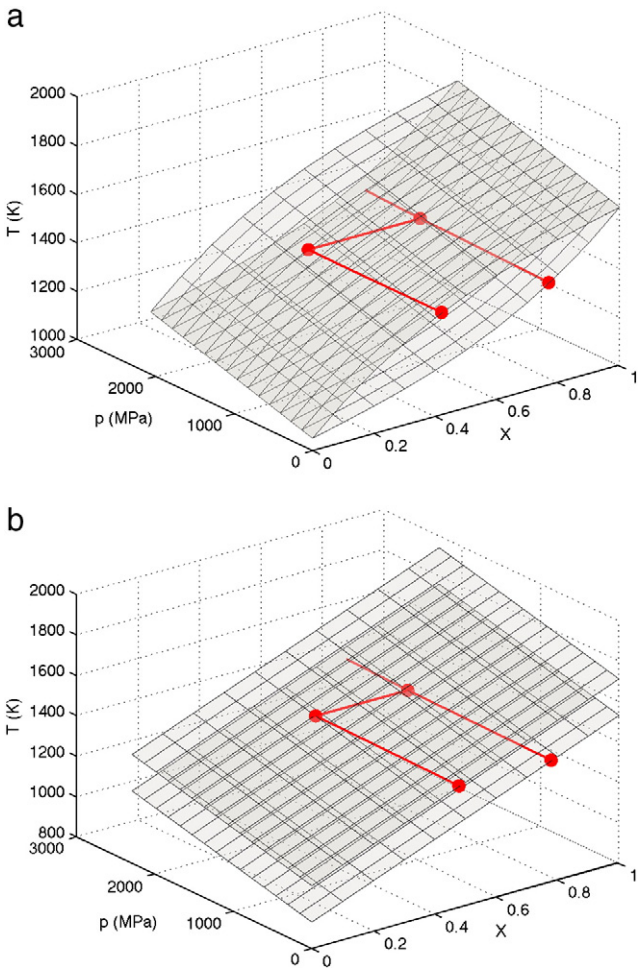

Fig. 2. (a) Liquidus and solidus given by Eqs. (1) and (2) with $f_L(X_l) = (X_l^3 + X_l)/2$ (the upper surface) and $f_S(X_s) = (X_s^3 - 3X_s^2 + 4X_s)/2$ (the lower surface), and with $\gamma = 10^{-7}\mathrm{KPa}^{-1}$, $\lambda = 600\mathrm{K}$ and $T_{L0} = T_{S0} = 1050\mathrm{K}$ (these illustrative forms for the solidus and liquidus are taken from (Katz, 2008)). The red line shows the melting path taken by rock with initial composition $X_m = 0.7$; as the rock ascends (ie. the pressure decreases) it reaches the solidus, and the tie linking the solidus and liquidus then gives the composition of the melt and residual matrix as it continues to ascend to the surface (see Fig. 3). (b) The same diagram for linear liquidus and solidus given by Eqs. (1) and (2) with $f_L(X_l) = X_l + \Delta X$ and $f_S(X_s) = X_s$, where $\Delta X = 0.3$, and with $T_{L0} = T_{S0} = 930$ K. (Color version online).

[1] Mantle potential temperature $\mathcal{T}$ is the temperature T corrected for adiabatic effects, so that $\mathcal{T}$ is the temperature the rock would be at if it were raised adiabatically to the surface $z=0$. See Eq. (13).

and solidus temperatures must be equal, and linking the two surfaces in Figure 2a with a tie shows how this determines a relationship between the solid and liquid compositions X_s and X_l. It may therefore be helpful to think of the phase constraints (1) and (2) in the form

$$T = T_{S0} + \gamma p_s + \lambda f_S(X_s), \quad X_l = K(X_s), \tag{3}$$

where $K(X_s)$ is the relationship between liquid and solid compositions, or, alternatively, to think of $T = T(p_s, F)$, where $F \equiv (X_s - X_m)/(X_s - X_l)$ is the degree of melting.

2.3. Conservation equations

Along with these phase constraints, the model requires conservation of mass and momentum for the two phases (solid matrix and liquid melt), conservation of each of the separate components within those phases, and conservation of energy. The general form of these equations is now relatively standard (McKenzie, 1984; Ribe, 1985b). We use as simple a description as possible, as the intention is to describe the essential dynamics of these regions, as I see them, rather than necessarily to provide the most realistic model possible. To this end, we make a Boussinesq approximation, assuming the densities of each phase are the same except in the buoyancy term. The model is then

$$\rho \frac{\partial \phi}{\partial t} + \rho \nabla \cdot [\phi \mathbf{u}] = m, \tag{4}$$

$$\nabla \cdot [(1-\phi)\mathbf{V} + \phi \mathbf{u}] = 0, \tag{5}$$

$$\rho \frac{\partial}{\partial t}[\phi X_l] + \rho \nabla \cdot [\phi \mathbf{u} X_l] = m^1, \tag{6}$$

$$\frac{\partial}{\partial t}[(1-\phi)X_s + \phi X_l] + \nabla \cdot [(1-\phi)\mathbf{V}X_s + \phi \mathbf{u} X_l] = 0, \tag{7}$$

$$p_s - p_l \equiv \mathcal{P} = -\frac{\eta_s}{\phi} \nabla \cdot \mathbf{V}, \tag{8}$$

$$p_s = -\rho g z, \tag{9}$$

$$\phi(\mathbf{u} - \mathbf{V}) = \frac{k_0 \phi^n}{\eta_l}(\Delta \rho g \mathbf{k} + \nabla \mathcal{P}), \tag{10}$$

$$mL + \rho c \frac{\partial T}{\partial t} + \rho[(1-\phi)\mathbf{V} + \phi \mathbf{u}] \cdot [c \nabla T + \alpha g \mathcal{T}_m \mathbf{k}] = 0. \tag{11}$$

Eqs. (4) and (5) represent overall conservation of mass. ϕ is the volume fraction of melt, ρ is the density (now approximated to be equal in solid and melt, whilst $\Delta\rho = \rho_s - \rho_l$ is the actual density difference), $\mathbf{u}$ is the melt velocity, $\mathbf{V}$ the matrix velocity, and m is the overall melting rate. Eqs. (6) and (7) represent conservation of the component making up fraction X_s of the matrix and X_l of the melt (together with Eqs. (4) and (5), this clearly ensures conservation of the other component too). m^1 is the rate of transfer of this component from matrix to melt ($m^2 = m - m^1$ is the equivalent rate for the other component). Diffusion of the components is neglected (though note this is *macroscopic* diffusion that is being neglected, on the basis that if we estimate the Péclet number we find it is very large. The assumption of thermodynamic equilibrium requires that diffusion on the *microscopic* scale of the pores *is* important, as maintaining equilibrium requires rapid transfer of components between the phases. The same is true for heat conduction discussed below).

The pressures in matrix and melt are p_s and p_l, but the latter is eliminated in favour of the effective pressure $\mathcal{P}$, defined as $p_s - p_l$. Eq. (8) is sometimes referred to as the compaction equation; it relates the pressure difference to the rate at which the porous matrix is able to compact as melt is extracted from it. The term η_s/ϕ is the bulk viscosity, often also written as ζ, and this form is motivated by simple microscopic models (eg. Bercovici and Ricard, 2003; Sleep, 1988).

Eq. (9) simply says that the matrix pressure is lithostatic, but is a simplification of the momentum equation for the whole system, in which a scaling analysis shows that the deviatoric matrix stress terms are expected to be small (Hewitt and Fowler, 2008). Eq. (10) is Darcy's law for the melt flux relative to the matrix. $k_0\phi^n$ is the porosity dependent permeability (with n taken to be 2 for the calculations in this paper), η_l is the melt viscosity, and the potential gradient driving the flow is $-\rho_l g \mathbf{k} - \nabla p_l$, which has been rewritten using Eqs. (8) and (9).

Finally, Eq. (11) is the energy equation, in which T is the temperature, L is the latent heat of melting (assumed constant), c is the specific heat capacity and α the thermal expansion coefficient (both assumed constant and equal in each phase). The adiabatic term $\alpha g T \mathbf{k}$ has been approximated by $\alpha g \mathcal{T}_m \mathbf{k}$ on account of the absolute temperature variation across the region being relatively small (the adiabatic term itself is in any case relatively small, so this is a fairly reasonable approximation). Heat conduction is neglected (see previous discussion).

Non-equilibrium models must prescribe the melting rates m and m^1, typically as some function of the 'distance' from equilibrium. In our case, assuming equilibrium, this is not necessary since the constraints posed by Eq. (3) will effectively determine what those rates must be. Indeed the main goal of this paper is to calculate the melting rate in this manner. Eqs. (4)–(11) together with Eq. (3) provide a closed system of 10 equations (in one dimension) for ϕ, m, $\mathbf{u}$, $\mathbf{V}$, X_l, X_s, m^1, p_s, $\mathcal{P}$, and T. Notice that m^1 appears only in Eq. (6), and it therefore decouples from the other equations.

The energy Eq. (11) has been written in terms of T because the phase constraints (3, and Fig. 2) are most easily interpreted in terms of T, p and X. It may be more natural, however, to consider Eq. (11) as an entropy equation (Asimow et al., 1997), which can be written in the conservation form

$$\frac{\partial}{\partial t}[(1-\phi)s_s + \phi s_l] + \nabla \cdot [(1-\phi)\mathbf{V}s_s + \phi \mathbf{u} s_l] = 0. \tag{12}$$

Here s_s and s_l are the specific entropies of the matrix and melt, and with the approximations outlined above they are related by $s_s - s_l \equiv \Delta s = -L/\mathcal{T}_m$ (the partial specific entropy difference as a result of compositional change at fixed T and p is ignored).

2.4. Depth of melting

Beneath the partially molten region, where the temperature is subsolidus, the same Eqs. (4)–(11) effectively still hold, but with $\phi = 0$, so that the only meaningful equations are the continuity Eq. (5) and temperature Eq. (11). Given the known upwelling velocity W_m and potential temperature $\mathcal{T}_m$, these imply $\mathbf{V} = W_m \mathbf{k}$ and the steady state adiabatic temperature profile[2]

$$T_a = \mathcal{T}_m - \frac{\alpha g \mathcal{T}_m}{c} z. \tag{13}$$

On the other hand, given the initial rock composition X_m, the solidus (Eq. (1)) also varies linearly with depth, and the depth at which melting starts, z_m, is therefore defined to be where T_a reaches T_S:

$$z_m = \frac{T_{S0} + \lambda f_S(X_m) - \mathcal{T}_m}{\gamma \rho g - \alpha g \mathcal{T}_m / c}. \tag{14}$$

[2] The approximation of the adiabatic term in Eq. (11) means this profile is linear rather than the usual exponential.

Table 1
Typical values of physical parameters used in the model.

g	$10\ \mathrm{ms}^{-2}$	L	$3\times10^{5}\mathrm{J\,kg}^{-1}$
ρ	$3000\,\mathrm{kg\,m}^{-3}$	c	$1000\,\mathrm{J\,kg}^{-1}\mathrm{K}^{-1}$
$\Delta\rho$	$500\,\mathrm{kg\,m}^{-3}$	α	$3\times10^{-5}\ \mathrm{K}^{-1}$
k_0	$4\times10^{-9}\ \mathrm{m}^2$	γ	$10^{-7}\mathrm{KPa}^{-1}$
η_l	10 Pa s	λ	600 K
η_s	10^{19} Pa s	$\mathcal{T}_m$	1480 K

Note that z_m should be negative; if Eq. (14) gives z_m positive it simply indicates that the rock remains below its solidus all the way to the surface and no partial melting occurs. Above this depth, for $z_m<z<0$, the full Eqs. (3)–(11) apply, and the boundary conditions are

$$\mathbf{V} = W_m\mathbf{k}, \quad \phi = 0, \quad X_s = X_m \quad \text{at} \quad z = z_m, \tag{15}$$

$$\mathcal{P} = 0 \quad \text{at} \quad z = 0, \tag{16}$$

the pressures being atmospheric at $z=0$. Since diffusion and conduction are ignored no further conditions on T or X at the boundaries are required.

2.5. Relative importance of terms

Based on the scaling that is conducted later and from geophysical inferences, we expect that the melt fraction ϕ will typically be small, on the order of perhaps 1%, but that the matrix is sufficiently permeable and the melt sufficiently buoyant that this allows melt velocity $\mathbf{u}$ to be much larger than the matrix velocity $\mathbf{V}$, perhaps $100\,\mathrm{cm\,y}^{-1}$ compared to $3\,\mathrm{cm\,y}^{-1}$.

The large melt velocity causes significant divergence of the melt from the matrix, which requires that the matrix compacts (due to mass conservation (Eq. (5))), and the effective pressure $\mathcal{P}$ needed to achieve this is given by Eq. (8). The typical size of this pressure turns out to be relatively small compared to the buoyancy term in Eq. (10); this is indicative of the fact that the *compaction length* is much less than the scale of the partial melting region (the compaction length is a natural length scale for these equations, and can be thought of as the length scale over which changes in pressure are accommodated by melt migration and matrix deformation. It depends upon permeability and therefore varies spatially with ϕ, but for a typical melt fraction ϕ_0 it is given by $\sqrt{k_0\phi_0^n\eta_s/\phi_0\eta_l}$). Typical values used for the parameters are given in Table 1.

3. One dimensional steady solutions

If we restrict solutions to a steady state in one dimension, most of the equations can be solved analytically, as is outlined in Appendix A (Ribe, 1985b). The melting process in this case is well known to be equivalent to isentropic batch melting of the source rock under the same pressure forcing (Asimow and Stolper, 1999). The main result is the expression

$$m = \rho W_m \frac{\partial F}{\partial z}, \tag{17}$$

for the melting rate m in terms of the degree of melting F. $F(z)$ is not *known*, however, and must be determined through energy conservation together with the phase constraints. As described in Appendix A, (11) can be integrated to give

$$LF + cT + \alpha g\mathcal{T}_m z = c\mathcal{T}_m, \tag{18}$$

which, together with Eq. (3), provides an algebraic system to solve for T, X_s, X_l and F as functions of z. The melting rate then follows from Eq. (17).

Figure 3 shows an example of the solutions using the form of the solidus and liquidus shown in Figure 2a. Solutions are shown for two different initial compositions X_m, and it is seen that these values have quite a large effect on the depth at which melting starts and on the degree of melting reached at the top of the column. The zero compaction length approximations in Eqs. (A.6)–(A.9) hold very well except in small boundary layers at the top and bottom of the melting region.

3.1. Linear phase constraints

It is noticeable that the variation of the melt and matrix compositions from their initial values where melting starts are quite small.

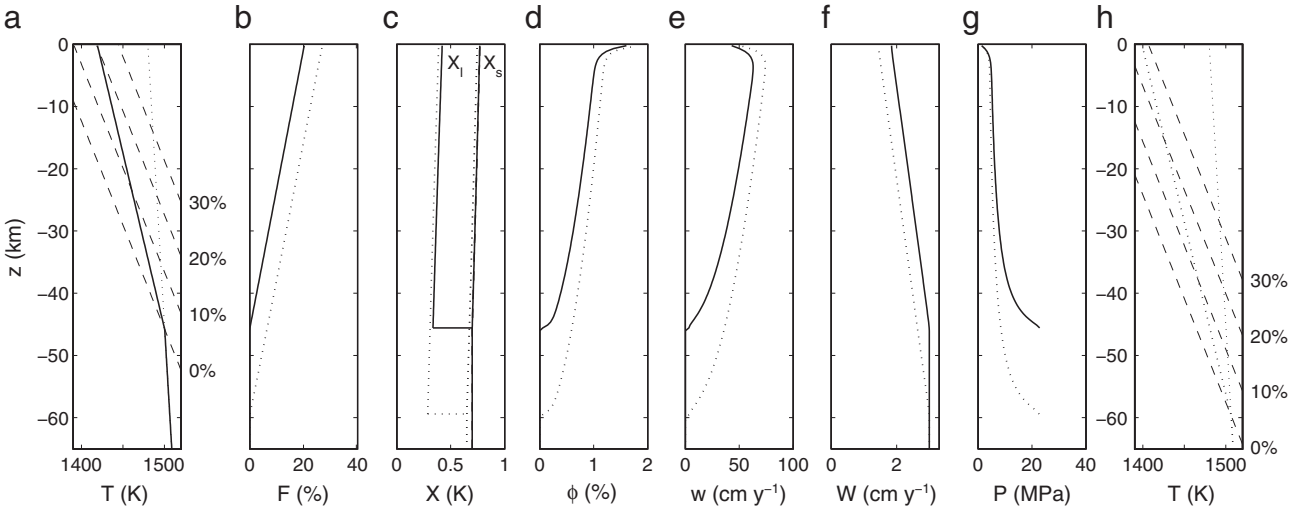

Fig. 3. Steady one dimensional solutions (solid lines) for (a) temperature, (b) degree of melting, (c) composition, (d) melt fraction, (e) melt velocity, (f) matrix velocity and (g) effective pressure, from Eqs. (4)–(11), with $W_m=3.2\,\mathrm{cm\,y}^{-1}$, $\mathcal{T}_m=1480\,\mathrm{K}$, $X_m=0.7$ and other parameters as in Table 1. The liquidus and solidus are as shown in Figure 2a, which also shows the same pressure–temperature–composition path taken by this rock. In (a), the dotted line shows the adiabatic path that would be taken if no melting occurred, and the dashed lines show the solidus for different degrees of melting (i.e. for different constant compositions relative to the initial composition X_m; their slope is the Clapeyron slope $\gamma\rho g$). The dotted lines in (b)–(g) show the solution for the same parameters except $X_m=0.65$, whilst (h) shows the temperature (as in (a)) for this dotted solution.

This motivates considering 'linearised' liquidus and solidus curves, such as in Figure 2b. These are written in the form of Eq. (3) as

$$T = T_{S0} - \gamma\rho g z + \lambda X_s, \qquad X_l = X_s - \Delta X. \tag{19}$$

The constant composition change ΔX can be seen as an analogue of the latent heat; when a small parcel of rock melts its heat changes by an amount ρL per unit volume, and its composition changes by an amount ΔX. This is of course a simplification, but arguably no more drastic than those already made in treating the rock as two components; in any case it allows for some mathematical simplifications without losing many important features of the dynamics.

The constraints (18) and (19) are then linear and are easily solved to give:

$$F = G(z - z_m), \quad \text{where } G = \frac{\gamma\rho g c - \alpha g \mathcal{T}_m}{L + c\lambda\Delta X}. \tag{20}$$

Thus, for linear dependence of the solidus and liquidus on composition, the degree of melting is found to vary linearly with depth, and the melting rate (Eq. (17)) is uniform, a constant multiple of the upwelling velocity.

This is not necessarily the case if different shapes of solidus and liquidus are assumed (although as seen in Figure 3 it may sometimes be approximately true), and Asimow et al. (1997) suggest that a uniform melting rate is quite unlikely in reality. Such a rate has often been assumed in the past, however (Ribe, 1985a; Sparks and Parmentier, 1991; Spiegelman, 1996; Spiegelman et al., 2001).

4. Melting rate for linear phase constraints

The previous section showed how the degree of melting and melting rate can be calculated straightforwardly for given phase constraints *assuming a one dimensional solution*; indeed the fact that melting is then equivalent to batch melting allows for significantly more complex and realistic calculations (Asimow and Stolper, 1999; Ribe, 1985b). Motivated by the simplicity of the solutions for the linear liquidus and solidus, however, we now maintain those constraints (19) and return to the full Eqs. (4)–(12) in more dimensions.

The entropy and composition equations can be written in this case as

$$-m\Delta s + \rho\frac{\partial s_s}{\partial t} + \rho[(1-\phi)\mathbf{V} + \phi\mathbf{u}]\cdot\nabla s_s = 0, \tag{21}$$

$$-m\Delta X + \rho\frac{\partial X_s}{\partial t} + \rho[(1-\phi)\mathbf{V} + \phi\mathbf{u}]\cdot\nabla X_s = 0, \tag{22}$$

and the linear phase constraints can be written in terms of entropy as

$$s_s = s_{s0} + \left(\frac{c\gamma}{\mathcal{T}_m} - \frac{\alpha}{\rho}\right)p_s + \frac{\lambda c}{\mathcal{T}_m}X_s, \tag{23}$$

where we have again judiciously approximated T by $\mathcal{T}_m$.

Combining these three equations and rearranging, we find

$$m = \rho[(1-\phi)\mathbf{V} + \phi\mathbf{u}]\cdot\mathbf{k}\,G, \quad G = \frac{\gamma\rho g c - \alpha g \mathcal{T}_m}{L + c\lambda\Delta X}. \tag{24}$$

This is the same as derived in the previous section except that the constant upwelling rate W_m is now replaced by the *average* rate $(1-\phi)W + \phi w$ (in one dimension mass conservation demands that this average velocity is equal to W_m).

This is a simple but important result that I want to emphasize. The overall melting rate is a constant multiple of the average upwelling velocity of both matrix *and* melt. Unlike Eq. (17) this allows for the possibility of non-uniform melting if there are regions where the porosities and velocities are different. The multiplying constant G depends upon the Clapeyron slope, the latent heat, and the compositional change of the solidus, with a small correction for adiabatic cooling. It is related to standard expressions for the *productivity*: $G/\rho g = -\partial F/\partial p$ (Asimow et al., 1997; McKenzie, 1984).

The expression only holds for the linear phase constraints in Figure 2b, but we might expect it to be approximately true for other phase constraints too. Notice that if we assumed a single component rock, so $\Delta X = 0$, Eq. (24) reduces to

$$m = \rho[(1-\phi)W + \phi w]\frac{c}{L}\left(\frac{\partial T_S}{\partial p} - \frac{\partial T_a}{\partial p}\right)\left(-\frac{\partial p}{\partial z}\right), \tag{25}$$

ie. melting rate depends only on the Clapeyron slope, as assumed by Hewitt and Fowler (2009) and Šrámek et al. (2007). If we were to ignore the temperature change and assume isothermal ascent then

$$m = \rho[(1-\phi)W + \phi w]\frac{1}{\Delta X}\frac{\partial X_l}{\partial z}, \tag{26}$$

ie. melting rate depends on the slope of the equilibrium composition, as typically assumed for studies of the reactive infiltration instability.[3]

4.1. Solutions for temperature and composition

Having used the entropy and composition equations with the phase constraints to calculate the melting rate, these equations then decouple from the remaining equations for ϕ, $\mathbf{u}$, $\mathbf{V}$ and $\mathcal{P}$. The temperature, composition and degree of melting are therefore independent of the flow dynamics. This is a peculiarity of the linear phase constraints; in general the entropy and composition equations must be solved at the same time as the remaining equations, together with the constraints, and the melting rate is determined as part of the overall solution (Katz, 2008). The constraints chosen here represent a special case in which a large part of the work can be bypassed by the calculation of m made above.

Substituting Eq. (24) into Eqs. (21) and (22), we see that $s_s - G\Delta s\, z$ and $X_s - G\Delta X\, z$ are constant on the streamlines of the mean velocity $(1-\phi)\mathbf{V} + \phi\mathbf{u}$. Hence, if the rock has uniform temperature $\mathcal{T}_m$ and composition X_m as it enters the column, these quantities are uniform everywhere, and the temperature, composition and degree of melting are given by the one dimensional solutions (see Eqs. (20), (A.11) and (A.12)). This will be the case even if the melting rate according to Eq. (24) varies in space, an apparently counter-intuitive result until it is remembered that melting is really driven by how fast rock moves down (up) the temperature (composition) gradient; the actual values of temperature and composition do not need to vary.

Since F follows the one dimensional solution, the melting rate (Eq. (24)) can be related to F as in Eq. (17), which is now generalized to

$$m = \rho[(1-\phi)W + \phi w]\frac{\partial F}{\partial z}. \tag{27}$$

[3] Note, however, that this assumes $X_s(z) = X_l(z) + \Delta X$, so that the equilibrium compositions of both matrix and melt vary with depth. If, like Liang et al. (2010), we assume $X_l(z)$ varies but X_s remains constant then $m^1 = mX_s$ and substituting into Eq. (6) gives

$$m = \rho\phi w\frac{1}{\Delta X}\frac{\partial X_l}{\partial z}.$$

Aharonov et al. (1995) and Spiegelman et al. (2001) make similar assumptions. If X_l and X_s both vary, but with different slopes, we find an intermediate case between this and Eq. (26), with the equilibrium slopes $\partial X_l/\partial z$ and $\partial X_s/\partial z$ weighted by the respective fluxes ϕw and $(1-\phi)W$.

4.2. Compaction equations for melt fraction and velocities

With the melting rate calculated as above, the remaining Eqs. (4), (5), (8) and (10) for ϕ, $\mathbf{u}$, $\mathbf{V}$, and $\mathcal{P}$, can be written in the dimensionless form

$$\frac{\partial \phi}{\partial t} + \phi_0 \nabla\cdot[\phi \mathbf{V}] + \phi \mathcal{P} = \mathcal{G}\Big[\mathbf{V} + \phi^n\Big(\mathbf{k} + \delta^2 \nabla \mathcal{P}\Big)\Big]\cdot\mathbf{k}.$$
$$\phi \mathcal{P} = \nabla\cdot\Big[\phi^n\Big(\mathbf{k} + \delta^2\nabla\mathcal{P}\Big)\Big] = -\nabla\cdot\mathbf{V}. \tag{28}$$

The variables have been scaled using the values defined in Table 2, as described in Appendix A. Besides the small porosity scale ϕ_0 there are two additional dimensionless parameters

$$\mathcal{G} = Gz_0 = \frac{\gamma\rho g c - \alpha g \mathcal{T}_m}{L + c\lambda\Delta X} z_0 \approx 0.25,$$
$$\delta^2 = \frac{\mathcal{P}_0}{\Delta\rho g z_0} = \frac{k_0\phi_0^n}{\eta_l}\frac{\eta_s}{\phi_0}\frac{1}{z_0^2} \approx 0.03. \tag{29}$$

$\mathcal{G}$ is the dimensionless version of the melting rate parameter G (it also therefore indicates the degree of melting at the top of the column), and δ is a dimensionless compaction length (*ie.* the ratio of the typical compaction length to the length scale z_0).

In two dimensions the original model (Eqs. (4)–(11)) does not actually provide enough information to solve for the full matrix velocity $\mathbf{V}$ (due to the neglect of the deviatoric stresses in Eq. (9)). We therefore follow the standard procedure of splitting $\mathbf{V}$ into incompressible and irrotational parts, and assume the former is prescribed entirely by the upwelling mantle flow. Thus

$$\mathbf{V} = W_m\mathbf{k} + \nabla\mathcal{U}, \tag{30}$$

where $\mathcal{U}$ is a velocity potential and W_m is the (now dimensionless) upwelling velocity.

The intention in the next section is to consider a two dimensional column and to examine the effect of perturbations in ϕ to the one dimensional solution. The advantage of using the linear phase constraints and calculating the melting rate explicitly is that we are left with a relatively simple set of Eq. (28) to study.

5. Reactive instability

Reactive instability can occur when the melting or dissolution rate increases with increasing melt flow. A common misconception is that it requires variations in composition (or temperature) between areas with larger and smaller porosity. This is not the case if equilibrium is assumed — as pointed out previously, it is the rate at which melt moves up the solubility gradient (or down the temperature gradient) which has to vary, and this is simply a result of the permeability increasing with porosity (if disequilibrium is allowed then of course the areas with larger porosity and larger melt flux will tend to be relatively undersaturated). Thus, although the temperature and the composition have been shown above to follow the one dimensional solutions, reactive instability is evidently a possibility.

Table 2
Definitions of scales used to non-dimensionalise the model, along with typical values using the parameters in Table 1.

Scale	Definition	Typical value	Units
V_0		3.2	$\mathrm{cm\,y^{-1}}$
z_0		50	km
m_0	$\frac{\rho V_0}{z_0}$	5.7×10^{-11}	$\mathrm{kg\,m^{-3}\,s^{-1}}$
ϕ_0	$\left(\frac{\eta_l V_0}{k_0\Delta\rho g}\right)^{1/n}$	0.022	
u_0	$V_0\left(\frac{\eta_l V_0}{k_0\Delta\rho g}\right)^{-1/n}$	140	$\mathrm{cm\,y^{-1}}$
t_0	$\frac{z_0}{u_0}$	3600	y
$\mathcal{P}_0$	$\frac{\eta_s}{\phi_0}\frac{k_0\phi_0^n}{\eta_l}\frac{\Delta\rho g}{z_0}$	8.7	MPa

5.1. Stability of a uniformly upwelling column

Consider the extension to two dimensions of the full melting column $z_m<z<0$ (z_m is now dimensionless, and should be approximately -1 with the right choice of length scale). The boundary conditions are (15) and (16), together with appropriate boundary conditions in the second dimension, which we denote y. Previous studies of reaction equations have tended not to look at this problem, instead concentrating on a region, presumably near the top of the column, where there is already some melt present. The inflow condition $\phi=0$ is then replaced by $\phi=\phi_{in}$, say, and an influx of melt is prescribed; this is discussed again later. The boundary condition at the top has also often been taken to be a 'free flux' condition, meaning $\partial\mathcal{P}/\partial z = 0$ there, but since this top boundary condition only affects a small $O(\delta^2)$ boundary layer near $z=0$ (see Fig. 3) this should not make a great difference, at least for small perturbations.

The steady one dimensional solution was found in Section 3. Denoting this by over-bars, and defining $Q=\phi(w-W)$ to be the vertical melt flux relative to the matrix, it is given approximately by Eqs. (A.6)–(A.9):

$$\mathcal{G}W_m \approx \overline{Q}\,(z-z_m), \quad \overline{W} \approx W_m - \overline{Q},$$
$$\overline{\phi} \approx W_m^{1/n}\mathcal{G}^{1/n}(z-z_m)^{1/n}, \quad \overline{\mathcal{P}} \approx \frac{W_m^{1-1/n}\mathcal{G}^{1-1/n}}{(z-z_m)^{1/n}}. \tag{31}$$

Since the background state depends on z in this way a linear stability analysis (such as studied by Aharonov et al. (1995) or Spiegelman et al. (2001)) is not straightforward. However two dimensional numerical solutions, taking as an initial condition the one dimensional profile with a small perturbation added to the melt fraction, indicate that it is stable for our typical values of n and $\mathcal{G}$. Small perturbations gradually diminish as the melt rises and the matrix compacts, and the solutions tend back to the steady one dimensional state.

Although a full mathematical stability analysis is not attempted here, we can understand this to some extent from the equations. Since diffusion is neglected and reactions are assumed to instantaneously maintain equilibrium (mathematically the model assumes the Péclet number and Damköhler number are infinite), we expect that the most unstable perturbations (if there are any) may be at the shortest lateral wavelength. If we seek local perturbations of the form $\mathcal{P} = \overline{\mathcal{P}}(z) + \mathcal{P}'\exp(\sigma t + iky)$ (and similarly for ϕ and $\mathbf{V}$), the two equations in Eq. $(28)_2$ indicate that for high wave numbers, $k\to\infty$, the perturbations $\mathcal{P}'$ and $\mathbf{V}'$ must be small (no z dependence is solved for; we consider only local perturbations so that the one dimensional state is approximately constant, which means boundary conditions in the z direction cannot be applied). The equation for ϕ' from Eq. $(28)_1$ then becomes

$$\sigma = n\mathcal{G}\overline{\phi}^{n-1}\left(1 + \delta^2\frac{\partial\overline{\mathcal{P}}}{\partial z}\right) - (1-2\phi_0\overline{\phi})\overline{\mathcal{P}}, \tag{32}$$
$$\approx \frac{n\mathcal{G}\overline{Q} - \mathcal{G}\left(\overline{W} + \overline{Q}\right)}{\overline{\phi}},$$

where the approximation ($O(\phi_0)$) is replacing the steady compaction term $\overline{\phi}\,\overline{\mathcal{P}}$ by the steady melt rate $\mathcal{G}\left(\overline{W}+\overline{Q}\right)$. This suggests that the steady state may be unstable ($\sigma>0$) if

$$n\overline{Q} \gtrsim \overline{W} + \overline{Q}, \tag{33}$$

and taking the approximations for $\overline{Q}$ and $\overline{W}$ in Eq. (31) this is

$$n\mathcal{G}W_m(z-z_m) \gtrsim W_m. \tag{34}$$

Since we take $n=2$, $\mathcal{G}\approx 0.25$ and $z-z_m \lesssim 1$, this condition is never satisfied and the steady state should be stable, as is found numerically. If we took $n=3$, it suggests instability might be possible near the top of the column if $\mathcal{G}\gtrsim 1/3$; we find numerically that it would require even larger $\mathcal{G}$, corresponding to more than 50% melting, which seems physically unlikely.

The approximate stability condition (33) has a simple interpretation. The driving mechanism for instability is that the melting rate increases with increasing melt flux. This is countered by compaction, which also increases when the melt fraction increases and therefore tends to stabilize small perturbations. The $n\overline{Q}$ term represents the increase in melting rate due to an increase in permeability, and the $\overline{W}+\overline{Q}$ represents the increase in compaction. Only if the melting rate dependence is strong enough (which requires that the background flux $\overline{Q}$ is large enough) can the system be unstable.

What, then, of the reaction infiltration instability? The equations studied here are admittedly simpler than those studied by, for instance, Aharonov et al. (1995) or Spiegelman et al. (2001) since they assume thermodynamic equilibrium and ignore diffusion, but this infinite Damköler number, infinite Péclet number limit ought to correspond to the *most* unstable cases considered there. The difference, I would argue, stems from the background state against which one perturbs.

5.2. Stability of a column supplied with melt

Previous studies of reactive infiltration have tended to take, as a base state, either a uniform porosity without any 'background' melting (*ie.* only including dissolution reactions driven by melt flow), or a situation with prescribed melting rate (proportional to W_m) in addition to the reactive dissolution, but in which there is already some melt present at the base of the column. The choice of these background states can completely change the stability properties.

As a comparison, consider the model in Eq. (28), but with altered boundary conditions

$$\mathbf{V} = W_{in}\mathbf{k}, \quad \phi = \phi_{in}, \quad Q = Q_{in}, \quad \text{at} \quad z = z_{in}, \tag{35}$$

where we are now considering a section of column $z_{in}<z<0$ in which there is already a quantity of melt ϕ_{in} present at the bottom, with melt flux Q_{in} there.

The approximate stability condition (33) still holds in this case, but the background states $\overline{Q}$ and $\overline{W}$ are now given by

$$\overline{Q} \approx Q_{in} + \mathcal{G}(W_{in}+Q_{in})(z-z_{in}), \quad \overline{W} \approx W_{in} + Q_{in} - \overline{Q}, \tag{36}$$

($\overline{\phi}$ and $\overline{\mathcal{P}}$ are similarly altered). Thus instability may occur if

$$n(Q_{in} + \mathcal{G}(W_{in}+Q_{in})(z-z_{in})) \gtrsim W_{in} + Q_{in}, \tag{37}$$

where the left hand side again represents the increase in permeability and therefore melting, and the right hand side represents the increase in compaction, as a result of a small change in melt fraction.

The formulation of the model used in this paper is such that the upwelling velocity W_{in} has more importance than in the studies of Aharonov et al. (1995) or Spiegelman et al. (2001), because it is what ultimately drives the melting rate and therefore determines the background state (its appearance in Eq. (37) is due to the melting term in Eq. $(28)_1$ rather than to the matrix advection term, which has been ignored as $O(\phi_0)$). For comparison with the results of those studies which ignore background melting however, we could take $W_{in}=0$, in which case Eq. (37) is always satisfied, since $n>1$.

Even if we allow $W_{in}>0$, Eq. (37) still suggests instability in this setup provided the influx Q_{in} is sufficiently large. Any of the previous mentioned studies which prescribe a fixed porosity or influx at the bottom of the domain have tended to satisfy this condition (though including diffusion and disequilibrium effects complicates whether one actually finds instability in that situation; note also that Eq. (33) is approximate and is only suggestive of instability).

Figures 4 and 5 show a numerical simulation of Eq. (28) with boundary conditions Eq. (35). This shows the time evolution of small random initial perturbations to the steady state which evolve over time to form a series of channels. Initially these grow at the scale of

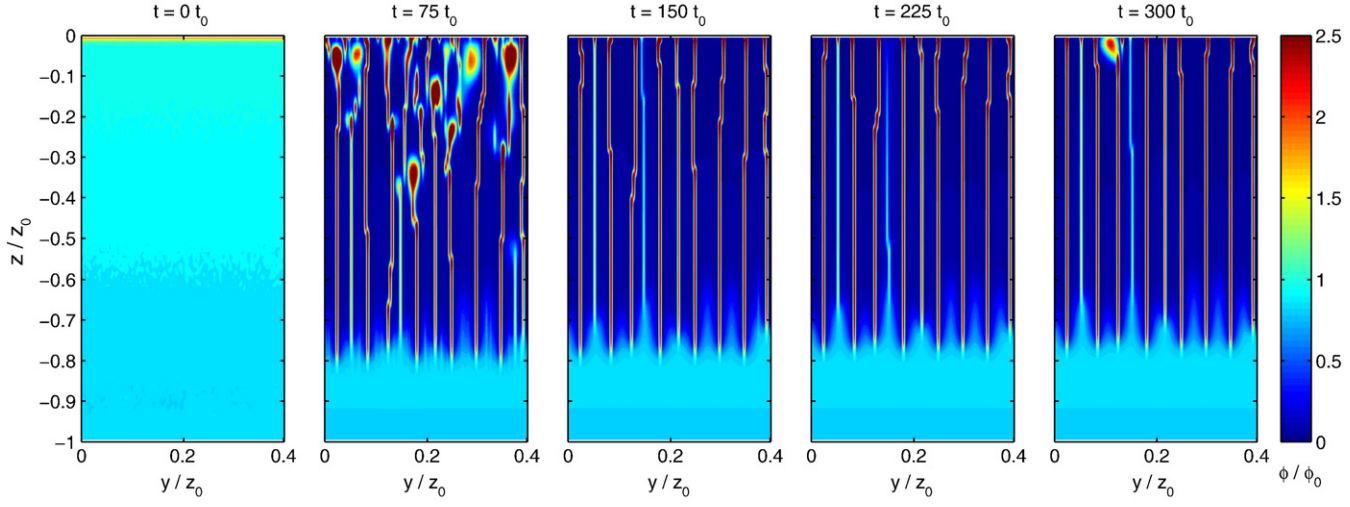

Fig. 4. Dimensionless solutions for ϕ of Eq. (28) with boundary conditions Eq. (35), and with initial condition consisting of the one dimensional steady state with additional random noise of dimensionless amplitude 10^{-2} at the grid scale. Dimensionless parameters are $\mathcal{G}=0.25$, $\phi_0=0.02$, $\delta^2=0.04$ and the bottom boundary conditions are $W_{in}=0.3$, $\phi_{in}=0.84$, $Q_{in}=0.7$. The colour scale stops at $\phi=2.5\phi_0$, but the melt fraction reaches up to 5 times of this at the top of some of the channels. The discretization is a rectangular grid which causes inaccuracies where channels change horizontal grid cells; since the channels evolve to be one cell wide, a different shape of grid would be required to avoid these. (Color version online).

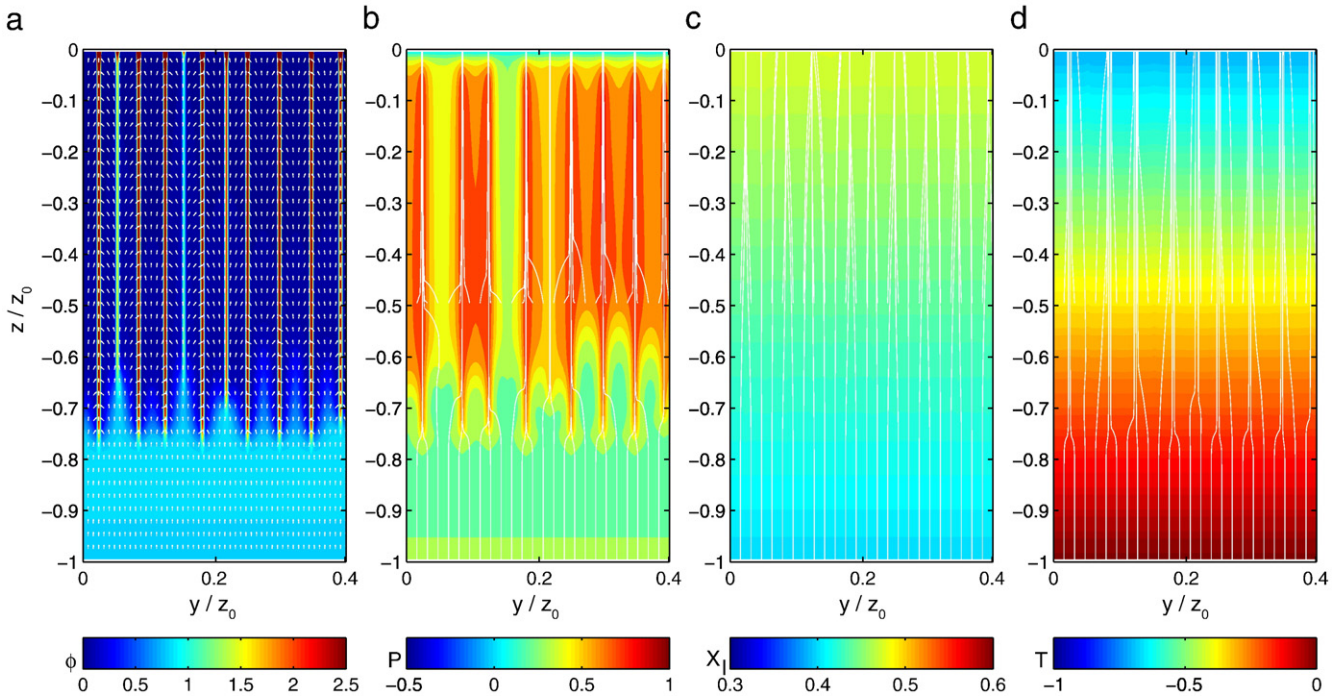

Fig. 5. Dimensionless solutions for (a) ϕ, (b) $\mathcal{P}$, (c) X_l, and (d) T, at the end ($t=500t_0$) of the run shown in Figure 4. The white arrows in (a) and the streamlines in (b) show the direction of the melt flow. The streamlines in (c) show the direction of the matrix flow, and the streamlines in (d) show the direction of the average velocity $(1-\phi)\mathbf{V}+\phi\mathbf{u}$. (For interpretation of the references to color in this figure legend, the reader is referred to the web version of this article.)

the discretization (presumably this would correspond physically to the grain scale), but they gradually coarsen to produce well defined channels (which are still only one grid cell wide) with larger intervening spaces of very reduced melt fraction. The spacing between the channels is determined by the compaction length, though it is noticeably less than that based on ϕ_0 (in the figure this is 0.2). This makes some sense since the compaction length in between the channels decreases substantially. The larger the imposed melt input Q_{in}, the deeper the channels extend into the melting region. The recent work of Liang et al. (2010) found similar results.

5.3. Channel growth

The channels that form in numerical solutions always evolve to be just one grid cell wide, no matter how fine the resolution. This is because the melt always wants to localise to the centre of a channel where the resistance is least and the melt pressure is therefore lowest. Similar behaviour is found in simulations of chimney formation in mushy layers (Katz and Worster, 2008), and it suggests that melt keeps localising until the melt fraction reaches 1. Indeed this is what occurs in the numerical solutions if the discretization is fine enough (though the solutions shown in this paper are not at sufficiently high resolution to achieve this). This means an open melt channel forms and the porous model is no longer appropriate there (in fact it probably loses validity long before ϕ reaches 1); an alternative model such as proposed by Hewitt and Fowler (2009) might be adopted for the channel.

5.4. Non-linear instability

Although we found that the full one dimensional column in Section 3 was not *linearly* unstable, it is still possible that a larger initial perturbation could grow by the same mechanism. A local increase in melt fraction causes an increase in the melting rate on the right hand side of Eq. $(28)_1$ and if this increase is sufficiently large to combat the simultaneous increase in compaction then the perturbation may grow.

Numerical solutions bear this out: for example, inserting a narrow band of cells with a porosity of 10% near the top of the melting region results in the melt fraction increasing in those cells, and enhanced melting as a result of the flow into the channel 'tip' causes it to extend downwards (into regions where the one dimensional solution was linearly stable). Very high resolution is needed to capture this growth, however, and the huge contrasts in permeability around the channel tip mean that a more sophisticated numerical method is needed to determine accurately how far and how fast such channels grow.

6. Discussion

6.1. Limitations of this model

The model presented here is highly simplified. It assumes that the rock is made up of only two components and that the solidus and liquidus temperatures depend linearly upon the concentration of those components, while a 'real' mantle rock is far more complex. The melting rate calculated in Eq. (27) made use of these specific thermodynamic relationships and will not necessarily hold in general. Nevertheless, to study the interaction between fluid flow and the melting process, this may be a useful simplification to make. It is certainly to be encouraged to use the average velocity $(1-\phi)W+\phi w$, rather than the upwelling velocity W_m, if prescribing a melting rate using that formula.

6.2. Instability and channelized flow

We have seen that the boundary conditions imposed at the bottom of a melting region are important. If it is supplied with enough melt, the results of the previous section suggest that dramatic channelization can occur. However, the amount of melt required is more than is predicted to be produced directly beneath that region, since the one dimensional solution for the *whole* column was found to be stable —

essentially there is not enough melt produced in the column to cause instability (there needs to be a sufficient quantity of melt for the flow dependence of the melting rate to become strong enough).

In the more realistic setting of a mid-ocean ridge, melt is expected to be drawn towards the ridge axis from a much wider region. It does not seem implausible to suppose that, at least near the top of the melting region, the 'upwelling column' beneath the ridge axis is supplied by considerably more melt than was produced directly beneath it (as predicted by the one dimensional model).

The observation that background melting can have a stabilizing effect is not new; Spiegelman et al. (2001) added a constant background melting rate to their simulations and found that this tended to reduce the channeling instability. The inclusion of the full melting process, and not just reactive melting is therefore important in assessing the instability. Indeed, it is not just reactive channelization that this is important for; Scott and Stevenson (1986) pointed out that melting tends to stabilize compaction waves (magmons) and emphasized the importance of including the melting process (Stevenson and Scott, 1991).

6.3. Bulk viscosity

The porosity dependence of the bulk viscosity is quite important in analyzing stability. For the short wavelength perturbations considered in the previous section, the stabilizing effect of compaction is due to the decrease in bulk viscosity that allows the matrix to compress more in regions of enlarged melt fraction. Spiegelman et al. (2001) adopt a bulk viscosity that becomes roughly constant for porosity larger than a 'compaction porosity' ϕ_c. Exploratory simulations using a similar form in the present model resulted in more unstable behaviour, but only if the compaction porosity is very small. Similarly, taking $\zeta = \eta_s/\phi^m$ results in the right hand side of Eq. (33) being multiplied by m, and hence the stronger the porosity dependence the greater the stabilizing effect.

6.4. Thermodynamic pressure

The pressure in the thermodynamic relationships (1)–(2) was taken for simplicity to be the lithostatic matrix pressure, whereas it should really be the thermodynamic or interfacial pressure. That is better approximated by the melt pressure (Fowler, 1985; McKenzie, 1984; Šrámek et al., 2007), in which case the solidus should have a small correction involving $\mathcal{P}$. Including this term would complicate the solution somewhat, but might lead to some interesting effects (see Hewitt and Fowler, (2008) for example).

6.5. Chemical variability

The assumption of thermodynamic equilibrium can aid the modelling of porous flow, and is quite well justified on the basis that typical estimates for the Damköhler number are large (Aharonov et al., 1995; Spiegelman and Kelemen, 2003; Spiegelman et al., 2001). It is not without issues, however, since a large part of the interest in channelised flow stems from the geochemical evidence to suggest that melt transport is often in disequilibrium. This obviously cannot be predicted or quantified using a model that implicitly assumes equilibrium. One must suppose that as the flow channelizes it reaches a stage when melt velocities in some places are so large that reaction and microscale diffusion are too slow to maintain equilibrium there (Spiegelman and Kenyon, 1992). This model would no longer be valid then, but for studying the initial stages of channel formation (and particularly whether channelization is possible) it provides a useful simplification. As noted earlier, allowing disequilibrium would tend to stabilize the system and make instability less likely. In particular, disequilibrium in a high-porosity channel would act to limit the melting rate and prevent the runaway opening of the channel that occurs here. A related point is that the solid matrix has been treated here as just one phase; if it were treated as two or more, with one more soluble than the others, exhaustion of that phase might limit the melting rate in a channel (Liang et al., 2010).

In the context of equilibrium melting, one can still consider the variations that might be expected in tracer concentrations in erupted melts (Spiegelman, 1996). For a trace element with a constant bulk partition coefficient κ, for instance, the concentrations in matrix and melt are related by $c_s = \kappa c_l$, and they satisfy the same conservation Eq. (7) as each of the major elements. With knowledge of the melt fraction and velocities, this equation can be solved for one of the concentrations, and an example is shown in Figure 6 for the unstable situation in Figure 4. This is the same type of behaviour as found by Spiegelman and Kelemen (2003): channels transport a larger tracer concentration and the melt in the regions between the channels is extremely depleted. The tracer element therefore bears the hallmarks of near-fractional melting in this case, whereas the major element compositions X were seen in Section 4 to be equivalent to batch melting.

6.6. Different types of perturbation

The investigation of stability in the previous section was limited to initial perturbations in melt fraction. Such heterogeneities are presumably common in partial melting regions, but it might be more natural to consider what happens if the supplied rock at the bottom of the column has a distribution of composition X_m that varies in space and perhaps time (similar perturbations in temperature are also a possibility, although it is more likely that heat conduction would have removed at least the small scale variations). I have not attempted to study this here because it introduces some added complexities. In particular, the depth z_m (Eq. (14)) at which melting begins varies with the initial composition and the melting region is no longer rectangular. A method that solves simultaneously for subsolidus and melting regions would be required.

One can gain some insight into what might happen in that case, however, from Figure 3. That figure shows the steady one dimensional solutions for two different initial compositions, $X_m = 0.7$ and $X_m = 0.65$, and one can consider what might happen if two such

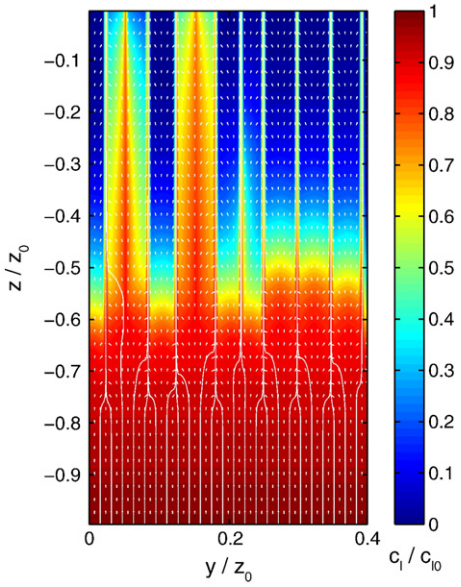

Fig. 6. Concentration in the melt (relative to the inflow concentration) of a tracer element with constant bulk partition coefficient $\kappa = 10^{-2}$ for the situation shown in Figure 5. White arrows and streamlines show the direction of melt flow. (For interpretation of the references to color in this figure legend, the reader is referred to the web version of this article.)

columns were side by side. The second one has a lower solidus temperature and therefore begins melting at a greater depth. The melt fraction in that column (the dotted line in the figure) is always larger than the melt fraction in the first column, and the melt flux is correspondingly higher. However, the effective pressure is *lower*, and one might therefore expect that the melt from this column would transfer into the first column (down the melt pressure gradient). This would act to even out the difference in melt fraction. A more thorough investigation would be worthwhile however, and heat conduction should also be included.

7. Conclusions

Including an energy equation and calculating the melting rate from conservation principles is an important ingredient in models of partially melting regions. Many models that account for the physics of melt migration have studied how melt that is present in the rock might move without incorporating the melting process; the conclusion of this paper is to emphasize that the nature of melt migration is intricately connected with the melting process. Background and reactive melting are not necessarily decoupled, and the melting process should therefore be considered as a whole.

The simplifications made in this paper allow the melting rate to be calculated explicitly, and found (Eq. (27)) that it is proportional to the average upwelling velocity and the gradient of the degree of melting.

The dependence of the melting rate on the melt velocity indicates the potential for reactive instability, and the model was shown to predict the growth of narrow high-porosity channels if there is a sufficient quantity of melt. If the melt flow dependence on the melting rate is too weak, however, the one dimensional solutions are stable. This was found to be the case for a uniform upwelling column with a reasonable choice of parameters, although the possibility for larger scale focusing of the melt may still provide sufficient melt to cause reactive instability in some areas.

Acknowledgment

I am grateful for the support of a Killam post-doctoral research fellowship at the University of British Columbia.

Appendix A. One dimensional steady solutions

In one dimension the matrix velocity is written as $W\mathbf{k}$ and the melt velocity is $w\mathbf{k}$. Integrating the steady state mass conservation Eqs. (5) and (7) together with the conditions $W=W_m$, $X_s=X_m$ and $\phi=0$ at $z=z_m$, give

$$W + \phi(w-W) = W_m, \tag{A.1}$$

$$(1-\phi)WX_s + \phi wX_l = W_mX_m, \tag{A.2}$$

and rearranging these shows that

$$\phi w = W_mF \equiv W_m\frac{X_s-X_m}{X_s-X_l}, \tag{A.3}$$

where F is the degree of melting. Substitution into Eq. (4) then gives the melting rate in terms of $F(z)$ in Eq. (17); in order to calculate $F(z)$, we substitute Eqs. (17) and (A.1) into the energy Eq. (11) and integrate, with T at $z=z_m$ given by Eq. (13), to find Eq. (18):

$$LF + cT + \alpha g\mathcal{T}_m z = c\mathcal{T}_m. \tag{A.4}$$

This is solved together with Eq. (3) and the definition $F=(X_s-X_m)/(X_s-X_l)$ to give T, X_s, X_l, and F as functions of z.

An alternative method is to use the entropy Eq. (12), which can be integrated to give

$$(1-F)s_s + Fs_l = s_m, \tag{A.5}$$

where s_m is the entropy of the upwelling rock at $z=z_m$, and this can be solved together with the entropy form of the phase constraints as in Eq. (23).

The solutions in Figure 3 are found in this way for the phase constraints in Figure 2a. ϕ, w, W and $\mathcal{P}$ are found numerically from Eqs. (4), (5), (8) and (10), but can be sensibly approximated by noticing that the matrix velocity is much smaller than the melt velocity in Eq. (10), and since the compaction length is small, this equation is $\phi w \approx k_0\Delta\rho g\phi^n/\eta_l$. Thus

$$\phi \approx \left(\frac{k_0\Delta\rho g}{\eta_l}\right)^{-1/n} W_m^{1/n}F^{1/n}, \tag{A.6}$$

$$w \approx \left(\frac{k_0\Delta\rho g}{\eta_l}\right)^{1/n} W_m^{1-1/n}F^{1-1/n}, \tag{A.7}$$

$$W \approx W_m(1-F), \tag{A.8}$$

$$\mathcal{P} \approx \eta_s\left(\frac{k_0\Delta\rho g}{\eta_l}\right)^{1/n} W_m^{1-1/n}F^{-1/n}\frac{\partial F}{\partial z}. \tag{A.9}$$

For the particular case of the linear solidus and liquidus (Eq. (19)) notice that, using the definition of z_m in Eq. (14), the solidus can be written in terms of F and z as

$$cT = c\mathcal{T}_m - \alpha g\mathcal{T}_m z_m - \gamma\rho gc(z-z_m) + c\lambda\Delta XF. \tag{A.10}$$

Substituting into Eq. (A.4) therefore gives $F=G(z-z_m)$, with G defined in the main text, and the temperature and composition are also then linear in z:

$$T = \mathcal{T}_m - \frac{\alpha g\mathcal{T}_m}{c}z - \frac{LG}{c}(z-z_m), \tag{A.11}$$

$$X_s(=X_l+\Delta X) = X_m + G\Delta X(z-z_m). \tag{A.12}$$

Appendix B. Non-dimensionalization

Using the expression for the melting rate in Eq. (24), the remaining Eqs. (4), (5), (8) and (10) become

$$\frac{\partial\phi}{\partial t} + \nabla\cdot[\phi\mathbf{u}] = G[\mathbf{V} + \phi(\mathbf{u}-\mathbf{V})]\cdot\mathbf{k}, \tag{B.1}$$

$$\frac{\phi\mathcal{P}}{\eta_s} = \nabla\cdot[\phi(\mathbf{u}-\mathbf{V})] = -\nabla\cdot\mathbf{V}, \tag{B.2}$$

$$\phi(\mathbf{u}-\mathbf{V}) = \frac{k_0\phi^n}{\eta_l}(\Delta\rho g\mathbf{k} + \nabla\mathcal{P}). \tag{B.3}$$

For Section 5 these are scaled using the parameter values defined in Table 2 (writing, for instance $\mathbf{V} = V_0\hat{\mathbf{V}}$, and then dropping the hats on the dimensionless variables) to arrive at Eq. (28). The depth of melting $-z_m$ and the upwelling velocity W_m are known *a priori*, and these provide the natural choice of length scale z_0 and velocity scale V_0. Since these quantities will differ between different rocks and different locations, however, we take z_0 and V_0 to be 'typical' values for them, and maintain the non-dimensional $-z_m$ and W_m in the equations. Although they could always be chosen to be 1, this makes it clearer, for instance, what the effect of a larger upwelling velocity is.

The choice of the remaining scales is motivated by balancing the following terms in the equations:

$$\phi u \sim \frac{k_0 \Delta\rho g}{\eta_l}\phi^n \sim V_0, \quad \mathcal{P} \sim \frac{\eta_s}{\phi}\frac{V_0}{z}. \tag{B.4}$$

The second of these indicates that the porosity scale ϕ_0 is chosen to balance melt flux $\phi\mathbf{u}$ with matrix flux $\mathbf{V}$. This is a somewhat arbitrary choice (an alternative is to choose ϕ_0 by balancing the melt divergence with the melting rate), but has the advantage of making the dimensionless equations appear particularly simple. The choice of scaling does not particularly matter, but it is helpful to choose one in which ϕ_0 is small (as is physically reasonable) to make clear which terms in the equations are important.

References

Aharonov, E., Whitehead, J.A., Kelemen, P.B., Spiegelman, M., 1995. Channeling instability of upwelling melt in the mantle. J. Geophys. Res. 100, 20433–20450.

Asimow, P.D., Hirschmann, M.M., Stolper, E.M., Nesbitt, R.W., 1997. An analysis of variations in isentropic melt productivity. Philos. Trans. R. Soc. Lond. A 255, 255–281.

Asimow, P.D., Stolper, E.M., 1999. Steady-state mantle–melt interactions in one dimension: I. Equilibrium transport and melt focusing. J. Petrol. 40, 475–494.

Bercovici, D., Ricard, Y., 2003. Energetics of a two-phase model of lithospheric damage, shear localization and plate-boundary formation. Geophys. J. Int. 152, 581–596.

Choblet, G., Parmentier, E.M., 2001. Mantle upwelling and melting beneath slow spreading centers: effects of variable rheology and melt productivity. Earth Planet. Sci. Lett. 184, 589–604.

Drew, D.A., 1983. Mathematical modeling of two-phase flow. Ann. Rev. Fluid Mech. 15, 261–291.

Fowler, A.C., 1985. A mathematical model of magma transport in the asthenosphere. Geophys. Astrophys. Fluid Dyn. 33, 63–96.

Hewitt, I.J., Fowler, A.C., 2008. Partial melting in an upwelling mantle column. Proc. R. Soc. A 464, 2467–2491.

Hewitt, I.J., Fowler, A.C., 2009. Melt channelization in ascending mantle. J. Geophys. Res. 114.

Ito, G., Mahoney, J.J., 2005. Flow and melting of a heterogenous mantle: 1. Method and importance to the geochemistry of ocean island and mid-ocean ridge basalts. Earth Planet. Sci. Lett. 230, 29–46.

Katz, R., Worster, M., 2008. Simulation of directional solidification, thermochemical convection, and chimney formation in a Hele-Shaw cell. J. Comput. Phys. 227, 9823–9840.

Katz, R.F., 2008. Magma dynamics with the enthalpy method: benchmark solutions and magmatic focusing at mid-ocean ridges. J. Petrol. 49, 2099–2121.

Kelemen, P.B., Hirth, G., Shimizu, N., Spiegelman, M., Dick, H.J.B., 1997. A review of melt migration processes in the adiabatically upwelling mantle beneath oceanic spreading ridges. Philos. Trans. R. Soc. Lond. A 355, 283–318.

Kelemen, P.B., Whitehead, J.A., Aharonov, E., Jordahl, K.A., 1995. Experiments on flow focusing in soluble porous media, with applications to melt extraction from the mantle. J. Geophys. Res. 100, 475–496.

Liang, Y., Schiemenz, A., Hesse, M.A., Parmentier, E.M., Hesthaven, J.S., 2010. High porosity channels for melt migration in the mantle: top is the dunite and bottom is the harzburgite and lherzolite. Geophys. Res. Lett. 37.

McKenzie, D., 1984. The generation and compaction of partially molten rock. J. Petrol. 25, 713–765.

McKenzie, D., Bickle, M.J., 1988. The volume and composition of melt generated by extension of the lithosphere. J. Petrol. 29, 625–679.

Ortoleva, P., Merino, E., Moore, C., Chadam, J., 1987. Geochemical self-organisation, II, the reaction–infiltration instability. Am. J. Sci. 287, 1008–1040.

Ribe, N.M., 1985a. The deformation and compaction of partial molten zones. Geophys. J. R. Astron. Soc. 83, 487–501.

Ribe, N.M., 1985b. The generation and composition of partial melts in the earth's mantle. Earth Planet. Sci. Lett. 73, 361–376.

Scott, D.R., Stevenson, D.J., 1986. Magma ascent by porous flow. J. Geophys. Res. 91, 9283–9296.

Scott, D.R., Stevenson, D.J., 1989. A self-consistent model of melting, magma migration and buoyancy-driven circulation beneath mid-ocean ridges. J. Geophys. Res. 94, 2973–2988.

Scott, D.R., Stevenson, D.J., Whitehead, J.A., 1986. Observations of solitary waves in a viscously deformable pipe. Nature 319, 759–761.

Sleep, N., 1988. Tapping of melt by veins and dikes. J. Geophys. Res. 93, 10255–10272.

Sparks, D.W., Parmentier, E.M., 1991. Melt extraction from the mantle beneath spreading centers. Earth Planet. Sci. Lett. 105, 368–377.

Spiegelman, M., 1993. Physics of melt extraction: theory, implications and applications. Philos. Trans. Phys. Sci. Eng. 342, 23–41.

Spiegelman, M., 1996. Geochemical consequences of melt transport in 2-D: the sensitivity of trace elments to mantle dynamics. Earth Planet. Sci. Lett. 139, 115–132.

Spiegelman, M., Kelemen, P.B., 2003. Extreme chemical variability as a consequence of channelized melt transport. Geochem. Geophys. Geosys. 4 (7), 1055. doi:10.1029/2002GC000336.

Spiegelman, M., Kelemen, P.B., Aharonov, E., 2001. Causes and consequences of flow organisation during melt transport: the reaction infiltration instability in compactible media. J. Geophys. Res. 106, 2061–2078.

Spiegelman, M., Kenyon, P., 1992. The requirements for chemical disequilibrium during magma migration. Earth Planet. Sci. Lett. 109, 611–620.

Šrámek, O., Ricard, Y., Bercovici, D., 2007. Simultaneous melting and compaction in deformable two-phase media. Geophys. J. Int. 168, 964–982.

Stevenson, D.J., 1989. Spontaneous small-scale melt segregation in partial melts undergoing deformation. Geophys. Res. Lett. 16, 1067–1070.

Stevenson, D.J., Scott, D.R., 1991. Mechanics of fluid–rock systems. Ann. Rev. Fluid Mech. 23, 305–339.

Stolper, E.M., Asimow, P.D., 2007. Insights into mantle melting from graphical analysis of one-component systems. Am. J. Sci. 307, 1051–1139.

Turcotte, D.L., Ahern, J.L., 1978. A porous flow model for magma migration in the asthenosphere. J. Geophys. Res. 83, 767–772.